

# Supernova 1998S at 14 years Postmortem: Continuing Circumstellar Interaction and Dust Formation

Jon Mauerhan<sup>1\*</sup> and Nathan Smith<sup>1\*</sup>

<sup>1</sup> *University of Arizona, Steward Observatory, Tucson, Arizona 85721, USA*

Submitted to MNRAS April 6 2012.

## ABSTRACT

We report late-time spectroscopic observations of the Type II<sub>n</sub> supernova (SN) 1998S, taken 14 years after explosion using the Large Binocular Telescope. The optical spectrum exhibits strong broad emission features of [O I], [O II], and H $\alpha$ , in addition to weaker features of [O III], H $\beta$  and [Fe II]. The last decade of evolution has exhibited a strengthening of the oxygen transitions relative to H $\alpha$ , evidence that the late-time emission is powered by increasingly metal-rich SN ejecta crossing the reverse shock. The H $\alpha$  luminosity of  $\approx 8000 L_{\odot}$  requires that SN 1998S is still interacting with relatively dense circumstellar material (CSM), probably produced by the strong wind of a red supergiant progenitor at least  $\sim 10^3$  years before explosion. The emission lines exhibit asymmetric blueshifted profiles, which implies that the receding hemisphere of the SN is obscured by dust. The [O III]  $\lambda 5007$  line, in particular, exhibits a complete suppression of its red wing. This could be the result of the expected wavelength dependence for dust extinction or a smaller radial distribution for [O III]. In the latter case, the red wing of [O III] could be absorbed by core dust, while both the blue and red wings are absorbed by dust within the cool dense shell between the forward and reverse shocks; this interpretation could explain why late-time [O III] emission from SNe is often weaker than models predict. The [O I] line exhibits double-peaked structure on top of the broader underlying profile, possibly due to emission from individual clumps of ejecta or ring-like structures of metal-rich debris. The centroids of the peaks are blueshifted and lack a red counterpart. However, an archival spectrum obtained on day 1093 exhibits a third, redshifted peak, which we suspect has become extinguished by dust that formed over the last decade, after day 1093. This implies that the “missing” red components of multi-peaked oxygen profiles observed in other SNe might be obscured by varying degrees of dust extinction.

**Key words:** supernovae: general — supernovae: individual (SN 1998S)

## 1 INTRODUCTION

Supernova (SN) 1998S, which occurred in the nearby host galaxy NGC 3877, is one of the most well-studied SNe of the core-collapse variety. It is designated a Type II<sub>n</sub>, a class which has raised critical new questions about the final phases of massive-star evolution. The “II<sub>n</sub>” designation refers to narrow emission lines of hydrogen observed in optical spectra (see Filippenko 1997), caused by relatively slow-moving circumstellar gas that is impacted by the blast wave or illuminated by UV radiation from the SN. The presence of these narrow lines requires dense circumstellar material (CSM) ejected by the progenitor star shortly (within a few years to decades) before the explosion. In some extreme

cases, up to  $25 M_{\odot}$  has been ejected in the decade before core collapse (Smith et al. 2007, 2008, 2010; Woosley et al. 2007), which has suggested a possible link to the class of eruptive luminous blue variables (LBVs). The impact of the SN blast wave on the CSM can efficiently convert kinetic energy into radiation, which explains why some Type II<sub>n</sub> events have been associated with several of the most luminous SNe yet recognized in the Universe, such as SN 2006gy (Smith et al. 2007, 2010; Ofek et al. 2007). In other less extreme cases, such as SN 1998S, SNe II<sub>n</sub> can exhibit interaction between the blast wave and a dense, but relatively-steady, hydrogen-rich wind from a red or blue supergiant progenitor. In all cases, long-term monitoring of the spectral evolution of Type II<sub>n</sub> SNe present the opportunity to probe the geometry, kinematics, structure, and chemistry of

\* E-mail: mauerhan@as.arizona.edu; nathans@as.arizona.edu

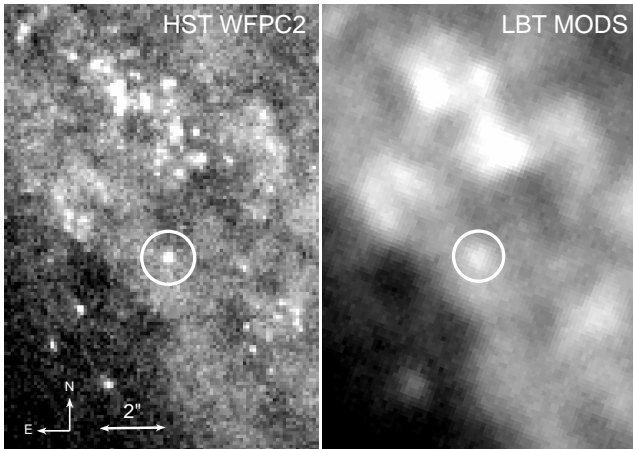


**Figure 1.** The local field of SN 1998S. The *HST*/WFPC2 image (F814W, *left*) is from 2000 Oct 1, and the LBT/MODS image (*g*-band; *right*) was obtained 2012 Jan 27.

both the slow-moving CSM and the rapidly expanding SN ejecta.

Early spectra of SN 1998S showed signs of CSM interaction very soon after explosion. Typical of Type II<sub>n</sub> evolution at early times, relatively narrow H $\alpha$  and He I emission lines exhibited broad Lorentzian wings, probably formed by electron scattering of photons diffusing out of the opaque pre-shock gas (Leonard et al. 2000; Chugai 2001; Fassia et al. 2001). Narrow P-Cygni profiles developed in the UV and optical spectra, generated by the slow-moving ionized stellar wind of the progenitor, which had an estimated velocity of 40–50 km s<sup>-1</sup> (Bowen et al. 2000; Fassia et al. 2001). At about 200 days, the H $\alpha$ , H $\beta$ , and He I lines began to exhibit complex structure in the form of asymmetric multi-peaked profiles, interpreted as the result of an expanding disk-like structure within the outflow (Leonard et al. 2000; Gerardy et al. 2000). SN 1998S also showed signs of thermal dust emission in the IR, either produced by the SN itself, thermal reprocessing of SN radiation by CSM dust, light echoes, or some combination of these (Fassia et al. 2000; Gerardy et al. 2002). The SN was also a strong long-lasting source of thermal X-rays, and generated radio free-free emission after about 300 days (Pooley et al. 2002), additional signposts of a lively CSM interaction.

An important question concerning SNe II<sub>n</sub> is how closely the eruptive pre-SN mass loss is linked to the impending core-collapse itself, or for how long before explosion the progenitor exhibited an unusually high mass-loss rate. For Type II<sub>n</sub> SNe, as well as for all other SNe that may explode into dense CSM, the impact of the blast wave upon the CSM can potentially manifest itself in observable characteristics that persist for decades. Such SNe, not necessarily classified specifically as Type II<sub>n</sub>, include 1957D, 1970G, 1979C, 1980K, 1986E, 1986J, 1993J, 1996cr, 1988Z, and of course SN 1987A (see Milisavljevic et al. 2012, and references therein). Here we present data obtained 14-years after explosion, which adds SN 1998S to this group of persistently interacting core-collapse SNe, and we discuss this object’s emission-line features in context.

## 2 OBSERVATIONS

SN 1998S was targeted for spectroscopic observation on 2012 Jan 27 (day 5079 after discovery) with the Multi-Object Double Spectrograph (MODS; Byard & O’Brien 2000) on the 8 m Large Binocular Telescope (LBT). Under  $\sim 0''.8$  seeing, a source at the SN position was detected in the 60.0 sec *r*-band target acquisition image, shown in Figure 1. From this image we were able to extract a photometric measurement using aperture photometry, deriving an *r*-band (SDSS) brightness of  $23.3 \pm 0.3$  mag.

Spectral images in the blue and red channels were obtained with MODS in longslit mode, utilizing the G670L grating and a  $1''.2$  slit, which yielded a spectral resolution of  $R \approx 1000$ . Because of guide star constraints, we had to observe the SN with the slit at  $\approx 45^\circ$  from the parallactic angle, prompting the concern that some blue light could have been lost as a result. However, since the SN was observed at an airmass of only  $\approx 1.1$ , and a  $1''.2$  slit was used under  $\approx 0''.8$  seeing, we do not expect substantial loss of blue flux. Four exposures totaling 80 min were obtained at the SN position.

The spectral images were bias subtracted, flat fielded, and median combined with a suitable rejection filter to remove cosmic rays. The spectrum was extracted using standard IRAF routines. Removal of the background line emission from the host galaxy required us to sample the background from a narrow strip very close to the dispersion track of the SN emission, such that the background region overlapped very slightly with the wings of the SN point spread function (PSF), but the result subtracted less than a few percent of the SN flux. The extracted spectrum was wavelength calibrated using spectra of HeNeAr lamps. The wavelength solution was corrected for the redshift of NGC 3877 ( $z = 0.003$ , Tully & Fisher 1988).

## 3 RESULTS

The new LBT/MODS spectrum of SN 1998S from day 5079 is shown in Figure 2, where it is compared to three earlier epochs from day 290, 474, and 1093 (archival spectra from Pozzo et al. 2004, obtained from the Weizmann interactive supernova data repository<sup>1</sup>; Yaron & Gal-Yam 2012). For days 290 and 474, only the range of the H $\alpha$  line is presented, since there was a lack of significant detections from other transitions at these epochs. Figure 3 shows our blue channel spectrum of SN 1998S and the earlier day 1093 epoch. For comparison, we included spectra of SN 1980K at 5509 days after discovery (Fesen et al. 1999; spectrum kindly provided by R. Fesen and D. Milisavljevic). Although the MODS wavelength coverage extends beyond the regions displayed in Figure 2, barely any continuum emission was detected on the latest epoch of SN 1998S outside of the displayed wavelength range. This insignificant amount of continuum is likely contaminated with background emission from the H II region that SN 1998S originated in, so we refrain from interpreting it.

The red channel spectra are dominated by strong, broad emission lines of H $\alpha$ , and the forbidden doublet transitions of [O I]  $\lambda\lambda 6300, 6364$  and [O II]  $\lambda\lambda 7319, 7330$ . There is also a

<sup>1</sup> [www.weizmann.ac.il/astrophysics/wiserep](http://www.weizmann.ac.il/astrophysics/wiserep)

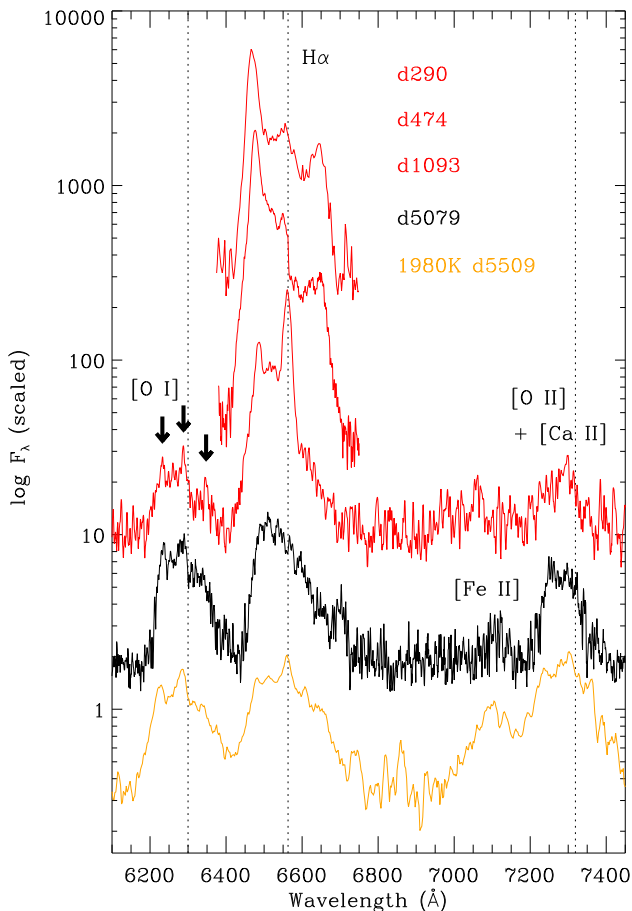


**Figure 2.** The LBT/MODS red channel spectrum of SN 1998S obtained 2012 Jan 27 (day 5079, *black*), compared with spectra of the same source on days 290, 474, and 1093 (*red*; Pozzo et al. 2004; Fassia et al. 2001). A spectrum of SN 1980K on day 5509 is also included for comparison (Fesen et al. 1999). On day 1093, the [O I] profile exhibited a triple-peaked narrow-component (*black arrows*), but the reddest of these has diminished by day 5079.

possible contribution from [Ca II]  $\lambda\lambda 7291, 7324$  which overlaps with [O II], although the latter is likely to be the dominant transition (Fesen et al. 1999). A weak but broad feature of [Fe II]  $\lambda 7155$  is also detected on the blue side of [O II], although [Ar III]  $\lambda 7136$  might be contributing to the flux as well.

The blue channel is dominated by [O III]  $\lambda 5007$  and  $H\beta$   $\lambda 4861$ , with the former exhibiting a dramatic cutoff of its blue wing. Weak [Fe II] emission is also present around  $\lambda 5100$ – $5200$ , where multiple transitions of this species lie.

Emission-line intensities, luminosities, and velocity parameters are listed in Table 1. The full-width at zero intensity (FWZI) of the  $H\alpha$  line is  $\approx 240$  Å, or  $\approx 11,000$  km s $^{-1}$ , while the oxygen lines have FWZI values closer to  $\approx 8000$ – $9000$  km s $^{-1}$ . For  $H\beta$  and [O III], the full extent of their respective red and blue wings is difficult to ascertain, because of the partial overlap of these lines. Luminosity calculations were made after applying foreground extinction and distance estimates of  $A_V = 0.68^{+0.34}_{-0.25}$  mag (Fassia et

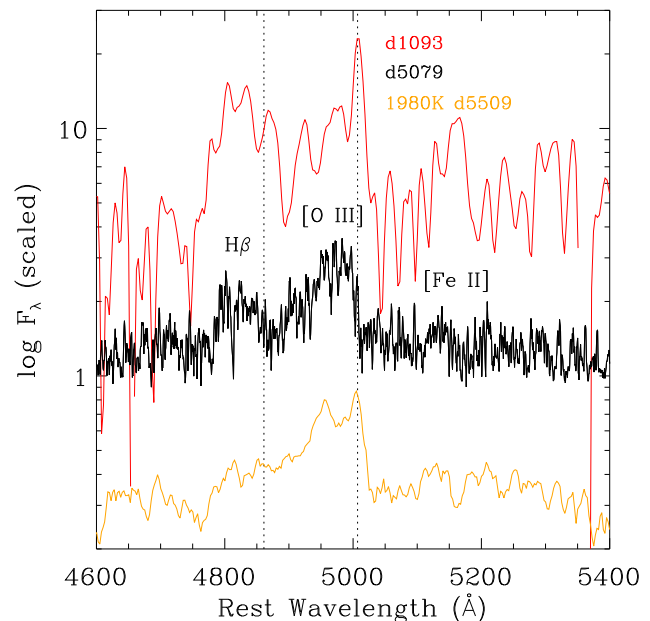


**Figure 3.** LBT/MODS blue channel spectrum of SN 1998S on day 5079 (*black*), compared to day 1093 (*red*, Pozzo et al. 2004), and SN 1980K 5509 days after discovery (*orange*, Fesen et al. 1999).

al. 2001) and  $15.5 \pm 1.3$  Mpc (NASA/IPAC Extragalactic Database [NED]), respectively. Extinction values were calculated for the rest wavelength of the emission line in question, assuming an extinction coefficient of  $R=3.1$  (Cardelli, Clayton, & Mathis 1989). No correction was made for the uncertain degree of internal extinction.

All of the line profiles exhibit asymmetric blueshifted peaks, probably the result of a suppression of flux on their red wings. The flux drop is particularly steep for [O III] and also for the central portion of the [O I] profile, with flux diminishing abruptly longward of their rest wavelengths.

There are conspicuous changes between day 1093 and 5079. Perhaps the most obvious are the disappearance of the intermediate-width, systemic-velocity components of the  $H\alpha$  line, and the increasing strength of oxygen emission with respect to  $H\alpha$ . Less obvious is the change in the triple-peaked profile of the [O I]  $\lambda\lambda 6300, 6364$  emission feature. The central peak, assuming it traces the  $\lambda 6300$  component of the doublet, appears blueshifted from rest by roughly  $-610$  km s $^{-1}$ , and the blue and red peaks are shifted by  $\approx -2600$  and  $+2800$  km s $^{-1}$ , respectively, from the central peak. It seems likely, although not certain, that each of these peaks represent different velocity components of the  $\lambda 6300$  transition of the doublet, since the underlying broad emission is centered near  $\lambda 6300$ , with no comparable broad emission centered near  $\lambda 6364$ . However, if the red peak is instead from the  $\lambda 6364$  component of the doublet, then it is exhibiting a blueshift of  $-800$  km s $^{-1}$ . Although the change is subtle, the central peak appears to become more sharply cutoff on its red side by day 5079. The blueshifted peak remains more or

**Table 1.** Line Measurements for SN 1998S on day 5079 ( $\approx 14$  yr). Luminosity errors are  $\approx 0.15$  dex, mainly dependent on distance and extinction uncertainties (day 2148 error is 0.25 dex, see text). Line ratios for the spectroscopically similar SNe 1980K and 1979C, at ages of 14–15 yr and 12–14 yr, respectively, are included for comparison (Fesen et al. 1999). Approximate luminosity ratios are given with respect to  $H\alpha$ . CF94 model predictions are included in the last column for power-law, and lower limits for RSG models.

Line	$\lambda_0$ (Å)	Intensity ( $\text{erg cm}^{-2} \text{s}^{-1}$ )	$\Delta V$ (edges) ( $\text{km s}^{-1}$ )	log $L$ ( $\text{erg s}^{-1}$ )	$L/L(H\alpha)$			
					(SN 1998S)	(SN 1980K)	(SN 1979C)	(CF94 model)
$H\beta$	4681	$6.3 \times 10^{-17}$	...	36.6	0.1	...	...	0.3
[O III]	4959, 5007	$1.3 \times 10^{-16}$	−5500, <100	36.9	0.3	0.1–0.2	0.9–1.1	3.4, >3.4
[O I]	6300 6364	$3.7 \times 10^{-16}$	−4500, 4000	37.3	0.6	0.7	0.9	0.6, >0.1
$H\alpha$	6563	$6.4 \times 10^{-16}$	−5500, 6000+	37.5	1	1	1	1
[Fe II]	7155	$3.5 \times 10^{-17}$	...	36.2	0.05	...	...	...
[O II]+[Ca II]	7319, 7330	$2.6 \times 10^{-16}$	−5500, 3500	37.1	0.4	0.9–1.0	11–12	0.4, >3.5

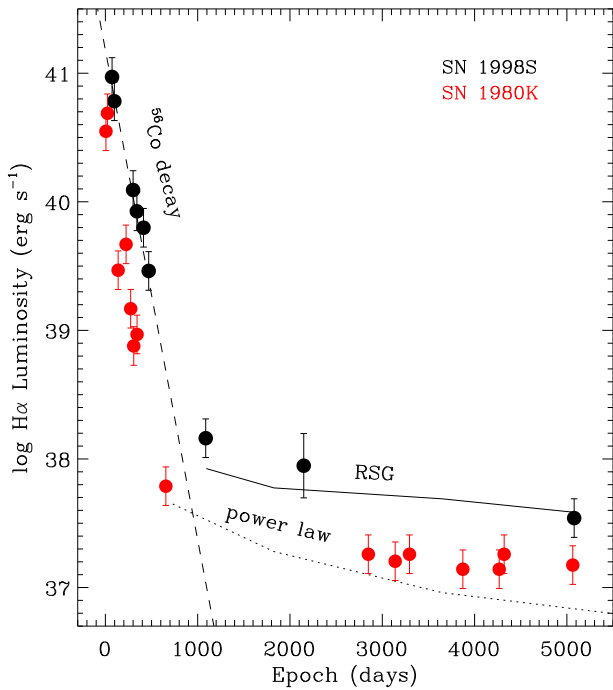


**Figure 4.**  $H\alpha$  luminosity curves for SN 1998S and SN 1980K. The luminosity at epochs <1000 days is consistent with the 111.5-day mean lifetime of radioactive  $^{56}\text{Co}$  (dashed line), but later epochs from day 1093 and onward fall above this trend by as much as 10 dex, requiring CSM interaction. The late-time luminosity of SN 1998S appears most consistent with model predictions for an RSG density profile (CF94; solid line), while SN 1980K lies between this and a power-law density profile (dotted line), as discussed in §4.

less unchanged. Remarkably, the reddest peak is no longer detected on day 5079.

The most recent epoch on day 5079 exhibits  $L(H\alpha) = (3.1 \pm 1.4) \times 10^{37} \text{ erg s}^{-1}$  ( $\approx 8000 L_{\odot}$ ). To compare this with past luminosity values, we adopted flux measurements from Fassia et al. (2001) and Pozzo et al. (2004) from day 1093 and earlier, and converted them to luminosities using the same distance and extinction values as before. In addition, an  $H\alpha$  flux for day 2148 was extracted from

a spectrum presented in Fransson et al. (2005; kindly provided by T. Matheson, but not shown here). The day 2148 spectrum was observed under poor seeing conditions. Thus, there was substantial and inseparable contamination from the background  $H\text{ II}$  region, specifically, narrow  $H\alpha$  and [N II]-doublet emission. We interpolated over these narrow features in order to estimate the broad underlying  $H\alpha$  flux of the SN. As a result, we may have removed some fraction of narrow  $H\alpha$  flux potentially intrinsic to the SN, if any were present at rest velocity on day 2148. In light of these caveats, we estimate a conservative error of 0.25 dex for the luminosity on day 2148. For additional comparison, we also include the  $H\alpha$  light curve for SN 1980K in Figure 4 (See Milisavljevic et al. 2012, and references therein), since this SN has exhibited spectral evolution very similar to SN 1998S, and has excellent late-time coverage. For SN 1980K, we adopted  $E(B - V) = 0.41$  mag (Fesen et al. 1999) and a distance of 6 Mpc (NED).

Earlier than 1000 days, the light curve for  $H\alpha$  is well matched by the radioactive decay trend of  $^{56}\text{Co}$  (111.5-day mean lifetime; Firestone et al. 1996). After 1000 days, the light curve departs from this trend, and hits a floor of  $\sim 10^{37.5} L_{\odot}$  that is maintained through day 5079. Since the day 5079 spectrum differs from the spectrum at early times, the late time  $H\alpha$  luminosity is not likely to be from an echo. Rather, the luminosity is accounted for by SN/CSM interaction, which we discuss in the following section.

## 4 DISCUSSION

### 4.1 Source of the Broad Line Emission

The collision between the SN explosion and the CSM can have lasting effects on the optical emission-line spectrum, long after the continuum has faded away. The impact of the SN blast wave on the CSM leads to the formation of a forward shock that meets the progenitor wind, and a reverse shock that gets bombarded by the expanding metal-rich SN ejecta (Chugai 1991; Chevalier & Fransson 1994, hereafter CF94). Gas in the cool dense shell (CDS) that develops between the forward and reverse shocks absorbs far-UV and X-ray photons generated within the shock, and this excites low-ionization transitions such as [Fe II] and [O I]. Inside the reverse shock, the hot outer layers of the metal-rich ejecta are also ionized, but give rise to higher ionization transitions, such as [O III] and UV metal lines. Both the CDS and

the ionized ejecta regions produce comparable amounts of  $H\alpha$ ,  $H\beta$ , and  $[O\ I]$  emission, while  $[O\ III]$  is generated almost exclusively on the skin of the ejecta, according to CF94. At late times ( $t > 10$  yr), the luminosity of the reverse shock becomes significantly higher than the forward-shocked CSM gas (by a factor of  $\approx 30$ , CF94). As the ejecta expands,  $[O\ I]$ ,  $[O\ II]$ , and  $[O\ III]$  emission are expected to increase relative to  $H\alpha$ , as collisional de-excitation becomes less effective for these forbidden transitions as the density drops.

CF94 provide predictions for the UV and optical emission-line luminosity that results from SN/CSM interaction. The luminosity of a given line depends on the ionizing luminosity of the reverse shock, which is sensitive to the density profile of the expanding supernova gas. This profile is, in turn, dependent on the stellar structure, the wind of the progenitor, and on the shock kinematics. CF94 consider the density profile of a red supergiant (RSG), which has relatively steep density gradients, in addition to more smooth power-law forms. The luminosity dependence of  $H\alpha$  can thus be expressed as

$$L(H\alpha) \propto \frac{L_s}{T_s} \propto \frac{V_s^3}{T_s} \left( \frac{\dot{M}}{v_w} \right), \quad (1)$$

where  $L_s$ ,  $T_s$ , and  $V_s$  are the shock ionizing luminosity, temperature, and velocity, respectively.  $\dot{M}/v_w$  is the wind density parameter, where the mass-loss rate and progenitor wind velocity are given in units of  $10^{-5} M_\odot \text{ yr}^{-1}$  and  $10 \text{ km s}^{-1}$ , respectively.

The  $H\alpha$  light curve for SN 1998S is shown in Figure 4, and includes model tracks for the SN density profile of a RSG and power-law distribution. The power law curve connects epochs 2, 5, 10, and 17 yr, adopted directly from CF94 (their Table 6); and the RSG curve was generated for epochs 3, 5, 10, and 14 yr by scaling the 10-yr  $H\alpha$  luminosity given in CF94 by the time-variable  $L_s/T_s$  ratio. Both models have  $\dot{M}/v_w = 5$ , which is an appropriate wind density parameter for SN 1998S, since the mass-loss rate and wind velocity of the progenitor have been estimated at  $40\text{--}50 \text{ km s}^{-1}$  and  $1\text{--}2 \times 10^{-4} M_\odot \text{ yr}^{-1}$  (Fassia et al. 2001; Pooley et al. 2002). The RSG and power-law CF94 models have ejecta velocities of  $4318$  and  $5038 \text{ km s}^{-1}$ , respectively. These velocities imply that 5079 days after explosion the shock should be located  $\sim 2 \times 10^{12} \text{ km}$  from the SN origin ( $\sim 13000 \text{ AU}$ ). Red supergiant winds extend to at least  $\sim 3 \times 10^{13} \text{ km}$  radius (Lloyd, O'Brien & Kahn 1995). Thus, the ongoing SN/CSM interaction during the most recent epoch is to be expected.

Overall, the late-time  $H\alpha$  luminosity trend of SN 1998S illustrated in Figure 4 is apparently most consistent with the RSG model. The  $H\alpha$  luminosity of SN 1980K, on the other hand, has late-time luminosity values  $\approx 6$  times lower than SN 1998S at similar epochs. The lower values could be explained as the result of the lower mass-loss rate of the SN 1980K progenitor ( $2.5 \times 10^{-5} M_\odot \text{ yr}^{-1}$ , Fesen et al. 1999), which is a factor of  $\approx 6$  lower than SN 1998S. As a result, the wind density parameter and, hence, the reverse shock luminosity for this object would also be lower by a comparable factor. Alternatively, the power-law density profile may be more consistent with SN 1980K, as argued by Fesen et al. (1999). However, although the RSG model is favored in the case of SN 1998S, it would be premature to overly discriminate between either models using line luminosities alone, since one only has to tweak the wind density parameter or

shock velocity to obtain a reasonable match to the data. It is also important to keep in mind that the luminosity could be affected by the highly uncertain degree of local extinction and/or asymmetries in emitting volume. If the ejecta or progenitor wind are asymmetric, the models we have considered here would be providing an underestimate of  $\dot{M}/v_w$  and  $L(H\alpha)$ . In any case, the implied mass loss rate of  $\sim 10^{-4} M_\odot \text{ yr}^{-1}$  for SN 1998S is extremely high, at the far upper end of the range exhibited by RSGs (Gehrz & Woolf 1971; Jura & Kleinmann 1990).

Elevated mass-loss rates could be a sign of impending core collapse for RSGs, perhaps driven by pulsation instabilities that generate a superwind (Yoon & Cantiello 2010). A suitable Galactic analog to the progenitor of SN 1998S could be the extraordinary object VY CMa (see Smith et al. 2001 and references therein). This RSG star is experiencing a very large mass-loss rate of  $\dot{M} = 2\text{--}4 \times 10^{-4}$  (with possible brief bouts as high as  $\sim 10^{-3} M_\odot \text{ yr}^{-1}$ ). It exhibits an average wind speed of  $30\text{--}40 \text{ km s}^{-1}$  and is surrounded by dense CSM that extends  $\sim 1000 \text{ AU}$  from the star, estimated to have been ejected over the last  $\sim 1000$  yrs. For these reasons, VY CMa has been highlighted as a viable SN II progenitor (Smith, Hinkle, & Ryde 2009a). For the progenitor of SN 1998S, the wind speed of  $40\text{--}50 \text{ km s}^{-1}$  combined with our estimated shock distance of  $13000 \text{ AU}$  implies that its high rate of mass loss began at least  $\approx 1200$  years before explosion. If this is close to the onset time for RSG superwinds (as suggested by Yoon & Cantiello 2010), and if the entering of this phase signifies a countdown to core collapse, it thus implies that VY CMa (whose superwind has been blowing for  $\sim 1000$  years) could explode relatively soon.

We observe an increase in oxygen emission relative to  $H\alpha$  over the last decade, providing evidence that the late-time emission traces increasingly metal-rich SN ejecta crossing the reverse shock (CF94). Between days 1093 and 5079 the  $[O\ I]/H\alpha$  ratio has increased from 0.1 to 0.6. This is roughly consistent with the power-law model and, to a lesser extent, the RSG model. However, over the same time period the  $[O\ III]/H\alpha$  ratio increased by a much smaller amount, from 0.2 to 0.3, which is an order of magnitude below the value predicted for the power-law model, and a factor of at least  $\approx 17$  below the RSG model. Serious discrepancies between the observed late-time line ratios and the CF94 model predictions, particularly regarding  $[O\ III]$ , have been reported for several other SNe observed at late times, including SN 1980K and 1979C (CF94; Fesen et al. 1999). The ratio is highly sensitive to the exact value of the shock velocity and the ejecta density. CF94 have suggested that a flatter density profile for the high-velocity ejecta, in addition to variations in shock temperature, could result in a lower ratio that would help resolve the discrepancy. Alternatively, the structure of the  $[O\ III]$  line profiles in SN 1998S and 1980K could be an indication that the optical depth of the  $[O\ III]$  emitting region beneath the reverse shock is larger than expected, which would also result in a lower observed line ratio; and we explore this possibility further below. The geometry and filling factor of the  $[O\ III]$  emitting region(s) could affect the result as well.

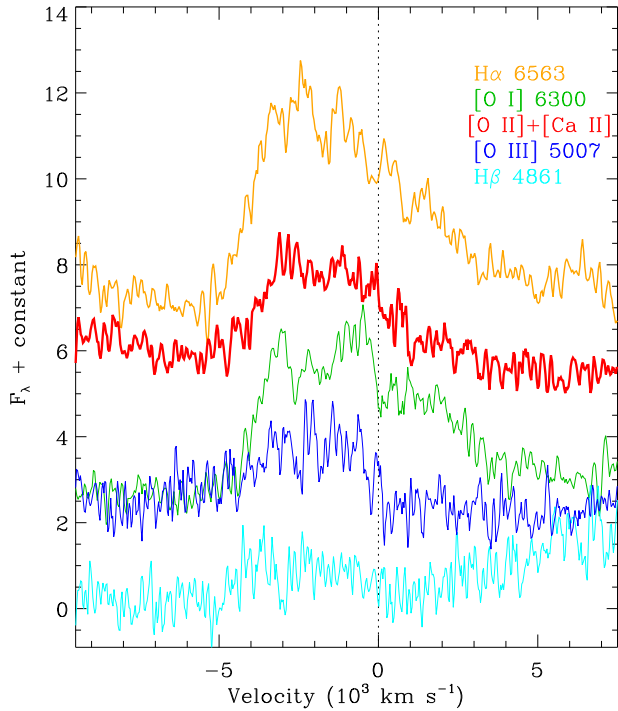


**Figure 5.** Velocity profiles for the strongest lines in the spectrum of SN 1998S. The shortest wavelength transitions, particularly [O I]  $\lambda$ 6300 and [O III]  $\lambda$ 5007, exhibit the most extreme flux cutoff on the red side of the line at zero velocity, strong evidence that internal dust extinction is the cause of the blue-shifted profiles. Note, the velocity of [O II]+[Ca II] should be taken with caution, since the center of the line blend could not be accurately determined.

#### 4.2 Line Profiles and Dust Extinction

The emission lines in the spectra SN 1998S exhibit substantial asymmetry and a net blueshift of their centroids. A commonly proposed explanation for this phenomenon is extinction by dust. In the case of SNe that interact with dense CSM, dust is expected to form in the cool dense shell (CDS) that develops between the forward and reverse shocks. Emission lines formed in the post-shock gas, exterior to the dusty CDS, will suffer little or no extinction, while the same emission features emerging from the receding hemisphere will be obscured by the dust. This results in the suppression of the red wings of the emission lines, causing a net blueshift. Dust formation in the CDS has been postulated to explain the spectral evolution of the Type II SNe 1980K, 1979C, 1993J, and 1999em (Dwek et al. 1983; Fesen et al. 1999; Wang & Hu 1994; Elmhamdi et al. 2003), the Type IIn SNe 2005ip and 2010jl (Smith et al. 2009b, 2012), and the Type Ib/Ibn SN 2006jc (Smith et al. 2008). Blueshifted emission lines have also been observed to develop in the spectra of core-collapse SNe that do not exhibit evidence for immediate interaction with dense CSM. In fact, SN 1987A was the first case to provide a convincing connection between the development of emission-line asymmetries and dust formation. After about day 500, a drop in optical flux was accompanied by a rise in IR emission; while around the same time, emission lines from SN 1987A began to exhibit asymmetry and blueshift

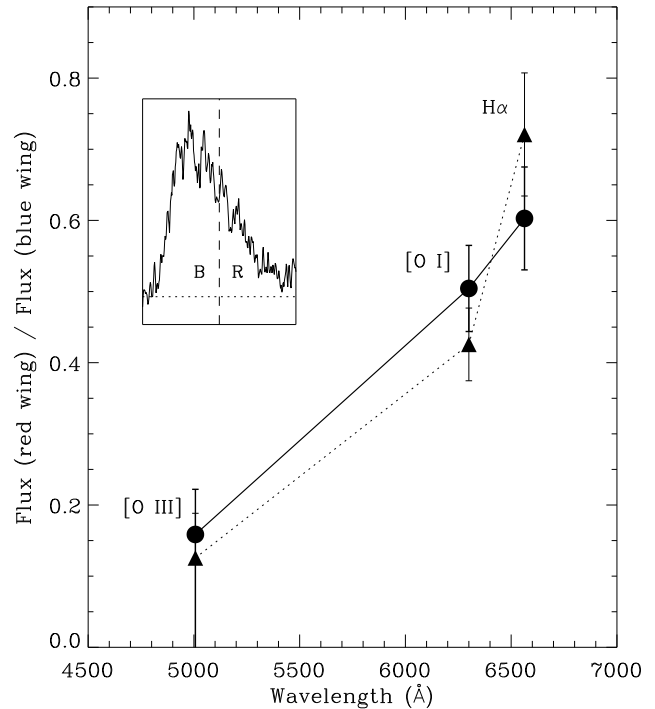


**Figure 6.** Ratio of the red-wing to blue-wing flux plotted against wavelength for SN 1998S (circles) and SN 1980K (triangles). The [O III] value for SN 1998S could be taken as an upper limit, since its red wing appears indistinguishable from pure continuum. The inset illustrates the blue and red wing regions of the H $\alpha$  line of SN 1998S, centered on the rest wavelength.

(Danziger et al. 1989; Lucy et al. 1989; Colgan et al. 1994; Wang et al. 1996). Similar phenomena was observed in the photometric and spectral evolution of SN 1990I (Elmhamdi et al. 2004). In these cases, however, dust formation likely occurred within the metal rich ejecta.

A large dust component has already been postulated in the case of SN 1998S. Gerardy et al. (2000) and Pozzo et al. (2004) monitored the NIR photometry and spectra between days 305–1242, observing the onset of CO emission and the development of a significant IR excess in the spectral energy distribution. These features could be attributable to thermal emission from dust synthesized in the SN, or IR echoes reflecting off of pre-existing dust clouds in the outer CSM (see Sugerman et al. 2012), or both. However, evolving asymmetry and increasing blueshift of the H $\alpha$  and He I  $\lambda$ 10830 lines observed by Pozzo et al. (2004) provided evidence that dust is likely being synthesized within the SN CDS.

The emission-line profiles of SN 1998S provide strong evidence for internal dust. Figure 5 provides a close-up of the most prominent lines plotted in velocity coordinates. All of the emission lines exhibit significant blueshift and appear suppressed on their red wings. Interestingly, a relatively abrupt drop in flux at zero velocity is observed for the two shortest wavelength transitions of oxygen. The effect is most extreme for [O III]  $\lambda$ 5007, which exhibits an apparently complete suppression of its red wing. Figure 6 shows the ratio of red-wing to blue-wing flux for [O III], [O I], and H $\alpha$  (H $\beta$  was excluded since [O III] overlaps with its red wing, and

[O II]+[Ca II] was excluded because the central wavelength of the uncertain line blend could not be accurately determined). The trend could possibly be the result of wavelength dependent extinction. The flux drop between H $\alpha$  and [O III] could imply a relative extinction ratio of  $\approx 1.4$  mag between  $\lambda 5007$  and  $\lambda 6563$ , which is consistent with an  $R \approx 3$  extinction coefficient for the obscuring material (Cardelli, Clayton, & Mathis 1989). However, we stress caution in drawing any definitive quantitative conclusions about the extinction law from the line profiles. In fact, the relative blue- and red-wing flux ratios from one atomic transition to another could be affected by differences in the radial distributions of the [O I], [O III], and H $\alpha$  emission zones. We discuss this further below.

#### 4.2.1 Evidence for Dust in the Unshocked Ejecta

The relative weakness of [O III] emission, and the complete suppression of its red wing imply some interesting possibilities for the distribution of obscuring dust within SN 1998S. Since the [O III] emission is expected to be generated exclusively on the outer skin of the unshocked ejecta (CF94), interior to the CDS and reverse shock, then we expect dust formed in the CDS will obscure both sides of this emission line equally. Thus, the large net blueshift of the [O III] emission line and the lack of a red wing require the obscuring material to be located interior to the [O III] zone, within the *unshocked* SN ejecta. If so, then practically the entire receding hemisphere of the [O III] emission skin would be obscured by dust in both the inner ejecta *and* in the CDS, explaining the lack of red wing flux. By comparison, the receding components of H $\alpha$  and [O I] emission, both of which can be generated at larger radii in the post-shock gas, and also potentially echoed by the CSM, would suffer less complete obscuration from inner ejecta dust, resulting in more red-wing flux for these lines relative to [O III]. Since both the blue and red wings of [O III] are absorbed by dust within the CDS, this could explain why late-time [O III] emission from SNe such as SN 1998S, 1980K, and 1979C, is often weaker than models predict (CF94; Fesen et al. 1999).

The spectrum of SN 1998S thus provides compelling evidence for dust formation in the CDS and within the unshocked ejecta. Dust formation in the latter zone has also been postulated in the cases of SNe 2005ip and 2006jc (Smith et al. 2008, 2009b). In addition, mid-infrared observations of the SN remnant 1E 0102.2–7219 in the Small Magellanic Cloud (Rho et al. 2009; Sandstrom et al. 2009) have provided evidence for the formation of dust within unshocked SN ejecta, interior to the [O III] emission zones.

### 4.3 Evolution of Multi-peaked Oxygen Profiles

The oxygen emission lines in the spectrum of SN 1998S exhibit interesting higher-order structure. Figure 7 shows a close-up of the [O I] emission feature on days 1093 and 5079. On day 1093, the line exhibits three narrow peaks with maxima at  $\lambda 6233$ ,  $\lambda 6287$ , and  $\lambda 6346$ , all on top of a broader underlying profile. By day 5079, the reddest of these peaks is no longer detected, leaving behind a double-peaked asymmetric profile having an overall blueshift, similar in appearance to SN 1980K on day 5509. As noted in §3, although we cannot

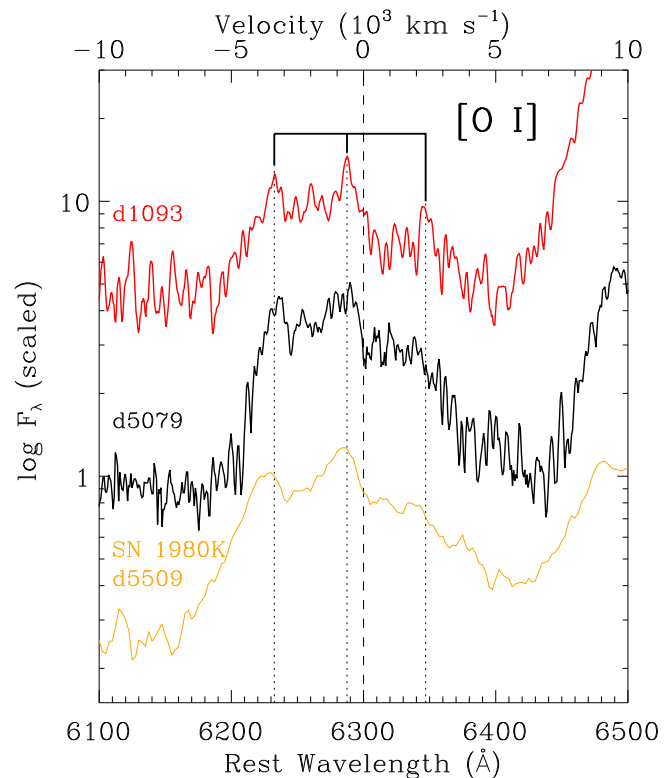


**Figure 7.** Close-up of the [O I]  $\lambda 6300$ ,  $\lambda 6364$  profile on days 1093 and 5079. The dashed line marks the rest wavelength of the  $\lambda 6300$  component of the transition. The dotted lines mark the center wavelengths/velocities of the triple peaks, assuming they all represent  $\lambda 6300$  (see caveats in text). SN 1980K on day 5509 exhibit very similar peak structure.

completely rule out the possibility that the reddest peak on day 1093 is a blueshifted  $\lambda 6364$  component of the doublet, we suspect that it actually represents a redshifted  $\lambda 6300$  component. Assuming this to be the case, the blue and red peaks would have velocities of approximately  $\pm 2600$ – $2700$  km s $^{-1}$  with respect to the central peak. The origin of these peaks and the cause of their temporal change is puzzling.

Double-peaked oxygen emission features have been observed in many other core-collapse SNe (e.g., see Modjaz et al. 2008, and references therein; Milisavljevic et al. 2009). One interpretation involves emission from large individual clumps of oxygen-rich ejecta (Wang & Chevalier 2002). However, this model could have difficulty explaining the apparent similarity of the wavelength spacing between peaks that is typically seen from one SN to another. Other interpretations include emission from the equatorial ring or torus of a bipolar outflow viewed nearly edge-on (Chugai & Danziger 1994; Maeda et al. 2008). However, the toroidal model always produces two peaks centered around the rest velocity, in addition to a possible central component. Milisavljevic et al. (2010) pointed out that the double-peaked oxygen profiles observed in core-collapse SNe (mainly Type Ib, IIb, and Ic) typically come in two main groups: *symmetric* profiles, where the trough between two peaks lies near rest velocity, with the peak separation lying conspicuously close to the 64 Å separation of the doublet components; and *asymmetric* profiles, where one component lies near rest and the other is blueshifted, having no conspicuous redshifted counterpart.

The [O I] profile of SN 1998S on day 5079 falls into the latter asymmetric category. On day 1093, however, the line appears more symmetric with the inclusion of the conspicuous red peak. The subsequent disappearance of this peak by day 5079 implies that it has been extinguished by dust, and therefore, originates from the receding hemisphere of the SN. This supports the interpretation that the peak is a redshifted  $\lambda 6300$  emission feature from the doublet, and not a blueshifted  $\lambda 6364$  feature.

We question whether the [O I] profile evolution could be related to the emergence and disappearance of the triple-peaked  $H\alpha$  profile at earlier times. By day 258, the  $H\alpha$  profile of SN 1998S exhibited a dramatic triple-peaked profile (see Figure 2). Its red and blue peaks were shifted by roughly  $\pm 4000 \text{ km s}^{-1}$  with respect to the central peak. Spectra from subsequent epochs exhibited a continuous flux decrease of the red peak, attributed to increasing extinction of the receding hemisphere of the SN by dust. By day  $\approx 650$  the red peak had become extinguished below detectability. The evolving red and blue peaks have been interpreted as the result of emission from an expanding ring or torus, with the central peak possibly arising from shocked circumstellar clumps (Gerardy et al. 2000; Leonard et al. 2000). However, Fransson et al. (2005) identified inconsistencies between this model and the observations, and instead favored a scenario in which double-peaked emission profiles emerge from a geometrically thin CDS behind the reverse shock, at large optical depth. Still, the CDS would probably have to be non-spherical to be consistent with the polarization measurements by Leonard et al. (2000). In any case, the observed evolution of the triple-peaked  $H\alpha$  profile motivates the following question. Could the triple-peaked structure of [O I]  $\lambda 6300$  seen on day 1093 — and the subsequent disappearance of its red component by day 5079 — be attributable to similar processes involving ring-like/toroidal ejecta or a non-spherical thin CDS, where the red peak of a corresponding triple-peaked profile eventually becomes extinguished as a result of persistent dust formation? Indeed, whatever structure the reverse-shock/CSM interaction exhibited at relatively early times would likely manifest again later as oxygen-rich ejecta eventually crosses over.

Disk, ring, and toroidal structures in SN ejecta have been suggested as viable explanations for observations of oxygen-rich SN remnants such as SNR 1E 0102.2–7219 in the Small Magellanic Cloud and Cassiopeia A in the Galaxy, both of which exhibit velocity structures indicative of asymmetric explosion geometries (Tuohi & Dopita 1983); indeed, the integrated spectra of the [O I]  $\lambda 6300$  line in Cassiopeia A exhibits a multi-peaked structure similar to what is seen in the spectra SN 1998S and 1980K (Milisavljevic et al. 2012). In addition, spectropolarimetry of other core-collapse SNe (Wang & Wheeler 2008, and references therein), the morphologies of many young Galactic remnants, and pulsar space velocity distributions (Cordes, Romani, & Lundgren 1993; Lyne & Lorimer 1994; Cordes & Chernoff 1998), collectively support the commonality of asymmetric explosions from core-collapse SNe.

## 5 CONCLUSIONS

Our observations of the IIn SN 1998S show that the CSM interaction is still going strong 14 years after explosion. The  $H\alpha$  luminosity has hit a slowly declining floor of  $L = 3.1 \times 10^{37} \text{ erg s}^{-1}$  ( $\approx 8000 L_{\odot}$ ). This behavior is very similar to SN 1980K, but indicates that the pre-SN mass-loss rate for the RSG progenitor of SN 1998S was extraordinarily high, even  $\approx 1200$  years before core collapse. This behavior suggests that other extreme RSGs, such as VY CMa, can potentially endure a similarly high degree of mass loss for at least 1200 years before exploding.

The blueshifted emission-line profiles observed from SN 1998S provide compelling evidence for the formation of dust. The relatively strong extinction of the red wing of the [O III]  $\lambda 5007$  line, in particular, is very interesting, as this is either a consequence of the wavelength dependence of the extinction, or the fact that the [O III] emission is generated exclusively interior to the shocks on the ionized skin of the inner ejecta, having its receding hemisphere completely obscured by inner core dust. Evidence for dust within the unshocked ejecta of SNe, interior to the [O III] emission zone, was acquired from mid-infrared observations of the SN remnant 1E 0102.2–7219 in the Small Magellanic Cloud (Rho et al. 2009; Sandstrom et al. 2009). Dusty O-rich remnants such as this could thus provide a glimpse at the possible appearance of SN 1998S and related SNe, centuries into the future.

Finally, the observed evolution of the multi-peaked [O I] profile, particularly the disappearance of the individual red peak, suggests that the red peak originated within the receding hemisphere of the SN and became obscured by dust that formed between days 1093 and 5079. The peak would therefore have to represent the  $\lambda 6300$  component of the doublet. This gives some credence to the interpretation that the individual peaks of oxygen profiles observed in other SNe represent emission features from separate structures within the outflow. This also implies that the “missing” conspicuous red peak in the multi-peaked [O I] profiles from other SNe might be the result of varying degrees of dust obscuration. Interestingly, SN 1998S must have formed significant amounts of dust after 3 years in order to extinguish the red peak between days 1093 and 5079.

## ACKNOWLEDGEMENTS

This research was based in part on observations made with the Large Binocular Telescope. The LBT is an international collaboration among institutions in the United States, Italy and Germany. The LBT Corporation partners are: the University of Arizona on behalf of the Arizona university system; the Istituto Nazionale di Astrofisica, Italy; the LBT Beteiligungsgesellschaft, Germany, representing the Max Planck Society, the Astrophysical Institute Potsdam, and Heidelberg University; the Ohio State University; and the Research Corporation, on behalf of the University of Notre Dame, University of Minnesota and University of Virginia. Our analysis utilized archival spectra of SN 1998S from the SUSPECT database. We thank T. Matheson, R. Fesen and D. Milisavljevic for providing earlier spectra of SN 1998S and 1980K for our comparison. We thank the referee Nikolai Chugai for insightful comments, which helped to improve the manuscript.



## REFERENCES

- Bowen, D. V., Roth, K. C., Meyer, D. M., & Blades, J. C. 2000, *ApJ*, 536, 225
- Byard, P. L., & O'Brien, T. P. 2000, *Proc. SPIE Vol. 4008*, 934
- Cardelli, J. A., Clayton, G. C., & Mathis, J. S. 1989, *ApJ*, 345, 245
- Chevalier, R. A., & Fransson, C. 1994, *ApJ*, 420, 268
- Chugai, N. N. 2001, *MNRAS*, 326, 1448
- Chugai, N. N., & Danziger, I. J. 1994, *MNRAS*, 268, 173
- Chugai, N. N. 1991, *MNRAS*, 250, 513
- Colgan, S. W. J., Haas, M. R., Erickson, E. F., Lord, S. D., & Hollenbach, D. J. 1994, *ApJ*, 427, 874
- Cordes, J. M., Romani, R. W., & Lundgren, S. C. 1993, *Nature*, 362, 133
- Cordes, J. M., & Chernoff, D. F. 1998, *ApJ*, 505, 315
- Danziger, I. J., Gouiffes, C., Bouchet, P., & Lucy, L. B. 1989, *IAU Circ.*, 4746, 1
- Dwek, E., A'Hearn, M. F., Becklin, E. E., et al. 1983, *ApJ*, 274, 168
- Elmhamdi, A., Danziger, I. J., Cappellaro, E., Della Valle, M., Gouiffes, C., Phillips, M. M. and Turatto, M. 2004, *A&A*, 426, 963
- Elmhamdi, A., Danziger, I. J., Chugai, N., et al. 2003, *MNRAS*, 338, 939
- Fassia, A., Meikle, W. P. S., Vacca, W. D., et al. 2000, *MNRAS*, 318, 1093
- Fassia, A., Meikle, W. P. S., Chugai, N., et al. 2001, *MNRAS*, 325, 907
- Fesen, R. A., Gerardy, C. L., Filippenko, A. V., et al. 1999, *AJ*, 117, 725
- Filippenko, A. V. 1997, *ARA&A*, 35, 309
- Firestone, R. B., Shirley, V. S., Baglin, C. M., Chu, S. Y. F., and Zipkin, J., *Table of Isotopes*, (the 8th edition; John Wiley & Sons, Inc., 1996)
- Fransson, C., Challis, P. M., Chevalier, R. A., et al. 2005, *ApJ*, 622, 991
- Gehrz, R. D., & Woolf, N. J. 1971, *ApJ*, 165, 285
- Gerardy, C. L., Fesen, R. A., Höflich, P., & Wheeler, J. C. 2000, *AJ*, 119, 2968
- Gerardy, C. L., Fesen, R. A., Nomoto, K., et al. 2002, *ApJ*, 575, 1007
- Jura, M., & Kleinmann, S. G. 1990, *ApJS*, 73, 769
- Lloyd, H. M., O'Brien, T. J., & Kahn, F. D. 1995, *MNRAS*, 273, L19
- Leonard, D. C., Filippenko, A. V., Barth, A. J., & Matheson, T. 2000, *ApJ*, 536, 239
- Lucy, L. B., Danziger, I. J., Gouiffes, C., & Bouchet, P. 1989, *IAU Colloq. 120: Structure and Dynamics of the Interstellar Medium*, 350, 164, Ed. Tenorio-Tagle, G., Moles M., and Melnick J., Springer-Verlag, Berlin, Heidelberg, New York
- Lyne, A. G., & Lorimer, D. R. 1994, *Nature*, 369, 127
- Maeda, K., Kawabata, K., Mazzali, P. A., et al. 2008, *Science*, 319, 1220
- Milisavljevic, D., Fesen, R., Chevalier, R., Kirshner, R., Challis, P., Turatto M., 2012, 751, 25
- Milisavljevic, D., Fesen, R. A., Gerardy, C. L., Kirshner, R. P., & Challis, P. 2010, *ApJ*, 709, 1343
- Milisavljevic, D., Fesen, R. A., Kirshner, R. P., & Challis, P. 2009, *ApJ*, 692, 839
- Modjaz, M., Kirshner, R. P., Blondin, S., Challis, P., & Matheson, T. 2008, *ApJL*, 687, L9
- Ofek, E. O., Cameron, P. B., Kasliwal, M. M., et al. 2007, *ApJL*, 659, L13
- Panagia, N., Vettolani, G., Boksenberg, A., et al. 1980, *MNRAS*, 192, 861
- Pooley, D., Lewin, W. H. G., Fox, D. W., et al. 2002, *ApJ*, 572, 932
- Pozzo, M., Meikle, W. P. S., Fassia, A., et al. 2004, *MNRAS*, 352, 457
- Rho, J., Reach, W. T., Tappe, A., et al. 2009, *ApJ*, 700, 579
- Sandstrom, K. M., Bolatto, A. D., Stanimirović, S., van Loon, J. T., & Smith, J. D. T. 2009, *ApJ*, 696, 2138
- Smith, N., Humphreys, R. M., Davidson, K., et al. 2001, *AJ*, 121, 1111
- Smith, N., Li, W., Foley, R. J., et al. 2007, *ApJ*, 666, 1116
- Smith, N., Foley, R. J., & Filippenko, A. V. 2008, *ApJ*, 680, 568
- Smith, N., Hinkle, K. H., & Ryde, N. 2009a, *AJ*, 137, 3558
- Smith, N., Silverman, J. M., Chornock, R., et al. 2009b, *ApJ*, 695, 1334
- Smith, N., Chornock, R., Silverman, J. M., Filippenko, A. V., & Foley, R. J. 2010, *ApJ*, 709, 856
- Smith, N., Silverman, J. M., Filippenko, A. V., et al. 2012, *AJ*, 143, 17
- Sugerman, B. E. K., Andrews, J. E., Barlow, M. J., et al. 2012, *ApJ*, 749, 170
- Tully R. B., & Fisher, J. R., 1988, *Nearby Galaxies Catalog*. Cambridge University Press, Cambridge
- Tuohy, I. R., & Dopita, M. A. 1983, *ApJL*, 268, L11
- Wang, L., Wheeler, J. C., Kirshner, R. P., et al. 1996, *ApJ*, 466, 998
- Wang, L., & Wheeler, J. C. 2008, *ARA&A*, 46, 433
- Wang, L., & Hu, J. 1994, *Nature*, 369, 380
- Wang, C.-Y., & Chevalier, R. A. 2002, *ApJ*, 574, 155
- Woosley, S. E., Blinnikov, S., & Heger, A. 2007, *Nature*, 450, 390
- Yaron, O., & Gal-Yam, A. 2012, arXiv:1204.1891
- Yoon, S.-C., & Cantiello, M. 2010, *ApJL*, 717, L62